Utrecht University

DEBYE INSTITUTE
NANOPHOTONICS GROUP
MASTER EXPERIMENTAL PHYSICS

Quasi-2D Optical Dipole Trapping of Bose-Einstein Condensates

Author:
Wouter Varenkamp BSc

Supervisors:
Prof. dr. Peter van der Straten
Jasper Smits MSc

30 July 2018

Abstract

The final stage in the creation of a Bose-Einstein condensate (BEC) is trapping and compressing in a strong magnetic trap. When the spin of an atom changes, it is lost from this magnetic trap. To be able to do experiments with varying atom spin, one can use an optical dipole trap, which traps atoms independent of their spin. This thesis presents a far red-detuned optical dipole trap, which is characterized by trapping BEC's. Furthermore, an approach to rapidly scan this trap is presented, creating a 'quasi-2D' potential. With this potential we attempt to create a horizontal sheet of condensed atoms, where the depth of the sheet of atoms is smaller than the range of the spin dynamics. This would enable a unique visualization of the spin dynamics using spin-dependent imaging.

Contents

1 Introduction

In 1995, a new state of matter was shown experimentally for the first time: the Bose-Einstein condensate (BEC). Eric Cornell and Carl Wieman were the first to create a BEC using rubidium atoms [1], followed in the same year by Wolfgang Ketterle using sodium atoms [2]. A BEC is formed by cooling a dilute gas of bosons to almost absolute zero temperature. At a certain critical temperature, the wavefunctions of the individual particles overlap to form a single quantum-mechanical state. The BEC is often referred to as the fifth state of matter, besides solid, liquid, gas and plasma.

To perform experiments based on the spin of the atoms in a BEC, a spin-independent trap is needed to hold the BEC. This thesis presents a red-detuned, focused Gaussian laser beam, which traps atoms relying on the induced dipole moment. This dipole moment interacts with the light field itselfs, pushing atoms towards higher intensities. These traps have a low optical excitation and are spin-independent. The theory of optical dipole traps is described in chapter 2. The optical setup used to create the trap is shown in chapter 3. The optical dipole trap is characterized by imaging the expansion of trapped BEC's. These expansion measurements and the trap characteristics are discussed in chapter 4.

Using spin-dependent imaging (SDI) [3], the spin-dynamics of a BEC can be visualized. By rapidly scanning the optical dipole trap, we attempt to create a quasi-2D horizontal sheet of BEC atoms. If the depth of the sheet of atoms is smaller than the range of the spin-dynamics, all the spin-dynamics happen in the horizontal direction of the sheet. The dynamics can be visualized using SDI. The scanning of the optical dipole trap is discussed in chapter 5. Finally, a conclusion and outlook are presented in chapter 6.

2 Theory

This chapter describes the theory of optical dipole traps in subsection 2.1, followed by the theory of trapped Bose-Einstein condensates in subsection 2.2. Equations from this chapter are used in chapter 4 to characterize the optical dipole trap.

2.1 Optical dipole trapping

Optical dipole trapping is based on the interaction of an atomic electric dipole moment with far-detuned light. This mechanism is much weaker than both magnetic and radiation-pressure trapping. An optical dipole trap is not limited by light-induced mechanisms present in radiation-pressure traps and is - under appropiate conditions - independent of the sub-level of the electronic ground state [4].

A light field $\mathbf{E}$ induces an atomic dipole moment $\mathbf{p}$ in an atom, which oscillates at a driving frequency ω. In complex notation we have

$$\mathbf{E}(\mathbf{r},t) = \hat{\mathbf{e}}\tilde{E}(\mathbf{r})(e^{-i\omega t} + e^{i\omega t}), \tag{1}$$

$$\mathbf{p}(\mathbf{r},t) = \hat{\mathbf{e}}\tilde{p}(\mathbf{r})(e^{-i\omega t} + e^{i\omega t}), \tag{2}$$

with $\hat{\mathbf{e}}$ the unit polarization vector. The dipole moment amplitude and light field amplitude are related by

$$\tilde{p} = \alpha\tilde{E} \tag{3}$$

where α is the complex polarizability. The induced dipole moment interacts with the light field. The interaction potential of the induced dipole moment is given by

$$U = -\frac{1}{2}\langle \mathbf{pE} \rangle = -\frac{1}{2\epsilon_0 c}\mathrm{Re}(\alpha)I. \tag{4}$$

The brackets denote a time-average and $I = 2\epsilon_0 c|\tilde{E}|^2$ is the field intensity. Following from the equation of motion of the driven oscillation, the polarizability can be written as

$$\alpha = 6\pi\epsilon_0 c^3 \frac{\Gamma/\omega_0^2}{\omega_0^2 - \omega^2 - i(\omega^3/\omega_0^2)\Gamma} \tag{5}$$

where Γ is the on-resonance damping rate and ω_0 the transition frequency. Using the expression for the polarizability of the atomic oscillator, equation (4) can be written as

$$U = -\frac{3\pi c^2}{2\omega_0^3}\left(\frac{\Gamma}{\omega_0 - \omega} + \frac{\Gamma}{\omega_0 + \omega}\right) I(\mathbf{r}). \tag{6}$$

The trap depth $\hat{U}$ is defined as $\hat{U} = |U(r = 0, z = 0)|$. The detuning is defined as $\Delta \equiv \omega - \omega_0$. For $\Delta < 0$, or "red" detuning, the dipole potential is negative. This means that the light field attracts atoms, with a potential minimum at the highest intensity. Therefore, the focus of a red detuned laser beam is a stable trap for atoms.

The intensity of a focused Gaussian laser beam along the z-axis is given by:

$$I(r, z) = \frac{2P}{\pi w(z)^2} \exp\left(-2\frac{r^2}{w(z)^2}\right), \tag{7}$$

with P the laser power, r the radial distance and $w(z)$ the waist, which can be written as

$$w(z) = w_0\sqrt{1 + \left(\frac{z}{z_R}\right)^2}. \tag{8}$$

Here w_0 is the beam waist of the focus and $z_R = \pi\omega_0^2/\lambda$, the Rayleigh length. When the thermal energy of the trapped atoms is much smaller than the trap depth $\hat{U}$, the extension of the atoms in both the radial and axial direction is small compared to the beam waist and Rayleigh length. The optical potential can be well aproximated by a cylindrically symmetric harmonic oscillator. This potential can be written as:

$$U(r, z) \approx -\hat{U}\left[1 - 2\left(\frac{r}{w_0}\right)^2 - \left(\frac{z}{z_R}\right)^2\right]. \tag{9}$$

A trapped atom oscillates in this potential with the following radial and axial frequencies:

$$\omega_\rho = \sqrt{\frac{4\hat{U}}{mw_0^2}}, \tag{10}$$

$$\omega_z = \sqrt{\frac{2\hat{U}}{mz_R^2}}. \tag{11}$$

2.2 Trapped Bose-Einstein condensates

The groundstate wavefunction of a Bose-Einstein condensate is defined as $\psi(\mathbf{r}, t) = \psi(\mathbf{r})e^{-i\mu t}$, where the groundstate energy is described by μ, the chemical potential of the condensate. This state is described by the following equation,

$$i\hbar\frac{\mathrm{d}\psi}{\mathrm{d}t} = -\frac{\hbar^2}{2m}\nabla^2\psi + U(\mathbf{r})\psi + \tilde{U}|\psi|^2\psi, \tag{12}$$

known as the Gross-Pitaevskii equation [5]. Here $|\psi|^2$ is the density, $\tilde{U} = 4\pi\hbar^2 a/m$ describes the effect of two-body collisions and a is the scattering length.

For a trapped condensate in the limit of strong interactions ($n\tilde{U} \gg \hbar\omega_{x,y,z}$), equation (12) can be simplified by neglecting the kinetic term. In this limit, known as the Thomas-Fermi limit, the density is described by:

$$n_c(\mathbf{r}) = \max\left(\frac{\mu - U(\mathbf{r})}{\tilde{U}}, 0\right). \tag{13}$$

The bottom of a dipole trap potential can be approximated as being harmonic. So we can describe condensates in the bottom of a trap by a parabolic density profile:

$$n_c(\mathbf{r}) = \frac{15}{8\pi}\frac{N}{\prod_{i=1}^{3} x_{i,c,0}}\max\left(1 - \sum_{i=1}^{3}\frac{x_i^2}{x_{i,c,0}^2}, 0\right). \tag{14}$$

In this equation $x_{i,c,0}$ are the half-lengths of the trapped condensate where the density goes to zero. The half-length of the condensate in the z-direction (or axial direction) is related to the axial trap frequency by:

$$\omega_z = \sqrt{\frac{2\mu}{m x_{z,c,0}^2}}. \tag{15}$$

From the chemical potential of a harmonically confined condensate in the Thomas-Fermi approximation, the relation between the radial trap frequency and the chemical potential is derived [5]:

$$\omega_\rho = \sqrt{\frac{(2\mu)^{5/2}}{15\hbar^2 m^{1/2} N_0 \omega_z a}}, \tag{16}$$

where N_0 is the number of atoms in the condensate, which can be determined by using absorption imaging. The half-length of the condensate in the axial direction, $x_{z,c,0}$, can also be determined by taking images of the condensate. The remaining parameter μ, the chemical potential, follows from the complete conversion of chemical potential to kinetic energy [6], such that

$$\mu = \frac{1}{2}mv^2. \tag{17}$$

By taking images of condensates at different expansion times, the expansion velocity v_{exp} can be determined. We can use this in equation (17) to calculate the chemical potential μ. Now everything is known to determine both ω_z and ω_ρ via equations (15) and (16). These can then be compared with the expected trap frequencies using equations (10) and (11). This is done in chapter 4.

3 Experimental setup

This chapter describes the experimental setup used to create Bose-Einstein condensates in section 3.1. In section 3.2 the setup of the optical dipole trap used to trap the BEC's is described.

3.1 Creating Bose-Einstein condensates

The creation of BEC's starts with melting sodium in an oven to create a beam of sodium atoms. These atoms are first slowed down in a Zeeman slower before being trapped in a Magneto-Optical Trap in the experimental chamber. The final step in the process is evaporative cooling in a strong magnetic trap to reach the critical temperature and form a Bose-Einstein condensate.

3.1.1 Oven

The first step in the process of creating a BEC is melting 20 - 30 grams of solid sodium in a stainless steel oven. The oven consists of two chambers. The first chamber contains the sodium and is heated to 300-315°C. It is connected to the second chamber by a 6 mm diaphragm, creating a beam of sodium atoms which passes into the second chamber. The second chamber has a temperature of approximately 100°C, just above the sodium melting point and another diaphragm of 10 mm which connects to the vacuum system. The atoms with the largest divergence are removed by this last diaphragm. The collimated beam passes through another 12 mm diaphragm before it enters the Zeeman slower. The flux of sodium atoms coming out of the oven is approximately $5 \cdot 10^{12}$ atoms/s.

3.1.2 Zeeman slower

The resulting atomic beam from the oven has a most probable velocity of approximately 600 m/s, with a spread described by the Maxwell-Boltzmann distribution. The Magneto-Optical Trap (MOT), however, has a capture velocity of around 50 m/s. The atoms are decelerated with a Zeeman slower using the momentum transfer of photons from an opposing laser beam. To keep the laser on the resonance frequency, the Doppler-shift due to the atoms velocity is compensated with a Zeeman shift induced by an inhomogeneous magnetic field along the direction of the atomic beam.

3.1.3 Magneto-Optical Trap (MOT)

The slowed atoms are captured in the Magneto-Optical Trap (MOT) in the experimental chamber. It consists of three orthogonal red detuned ($\delta = -1.5\Gamma$) laser beams, which are reflected back in the opposing directions, ensuring cooling in all directions. The laser beams are combined with a spatially dependent magnetic quadrupole field. The magnetic field induces a Zeeman shift in the atoms, which increases radially from the center. Atoms moving away from the center are now more likely to absorb a photon and are pushed to the center.

The resulting temperature of the cloud of atoms in the MOT is approximately 200 μK.

3.1.4 Magnetic Trap

To reach the limit where the atoms form a BEC evaporative cooling in a magnetic trap (MT) is used. In the MOT, the atoms are equally divided among three magnetic sub-states ($F_g = 1, m_f = -1, 0, 1$). The MT only traps the $m_f = -1$ state atoms, a third of the total number of atoms in the MOT. To increase this fraction, the atoms are spin-polarized by a strong magnetic field and pumped to the $m_f = -1$ state before being transferred to the MT. The next step is forced evaporative cooling using a radio-frequency (RF) field. The field spin flips atoms with the highest energy from the ($F_g = 1, m_f = -1$) to the ($F_g = 1, m_f = 0, 1$) state, removing them from the trap. By removing the highest energy atoms, the remaining atoms reach the critical temperature of $\approx$1 μK, forming a BEC.

3.2 Optical dipole trap setup

3.2.1 Optical setup

Figure 1 shows the setup used for creating an optical dipole trap. A 5 watt infrared laser[1] beam (1064 nm) passes through a telescope consisting of a +40mm and a +50mm lens for collimation and a small beam expansion. The resulting beam width is slightly smaller than the active aperture size of the AOM[2] it passes next.

The driver of the AOM is connected to two arbitrary waveform generators[3], one controlling the AOM frequency and one controlling the AOM amplitude. After passing a +50mm lens behind the AOM the 0-th order is directed into a beam dump, whilst the 1-th order is picked off near the focus using a D-shaped mirror. The +50mm lens in combination with the +500mm lens expands the beam with a factor of 10. The beam is finally focused into the experimental chamber using a +300mm lens, resulting in a waist size of approximately 11 μm and a Rayleigh length of 357 μm. The final lens is mounted on a stage to be able to adjust the distance from the experimental chamber and therefore the z-position of the focus in the chamber. The focus can be imaged onto a CCD camera using the folding mirror behind the final lens.

Behind the experimental chamber a +200 mm lens focuses the beam into a beam dump. A glass plate splits a part of this focused beam and images it onto another CCD camera. This camera is used to determine the (x, y) position of the laser focus in the chamber. By using fluorescence of the atomic cloud, its

[1] IPG Photonics YLM-5-LP-SC
[2] ISOMET M1135-T80L-3
[3] Agilent 33509B

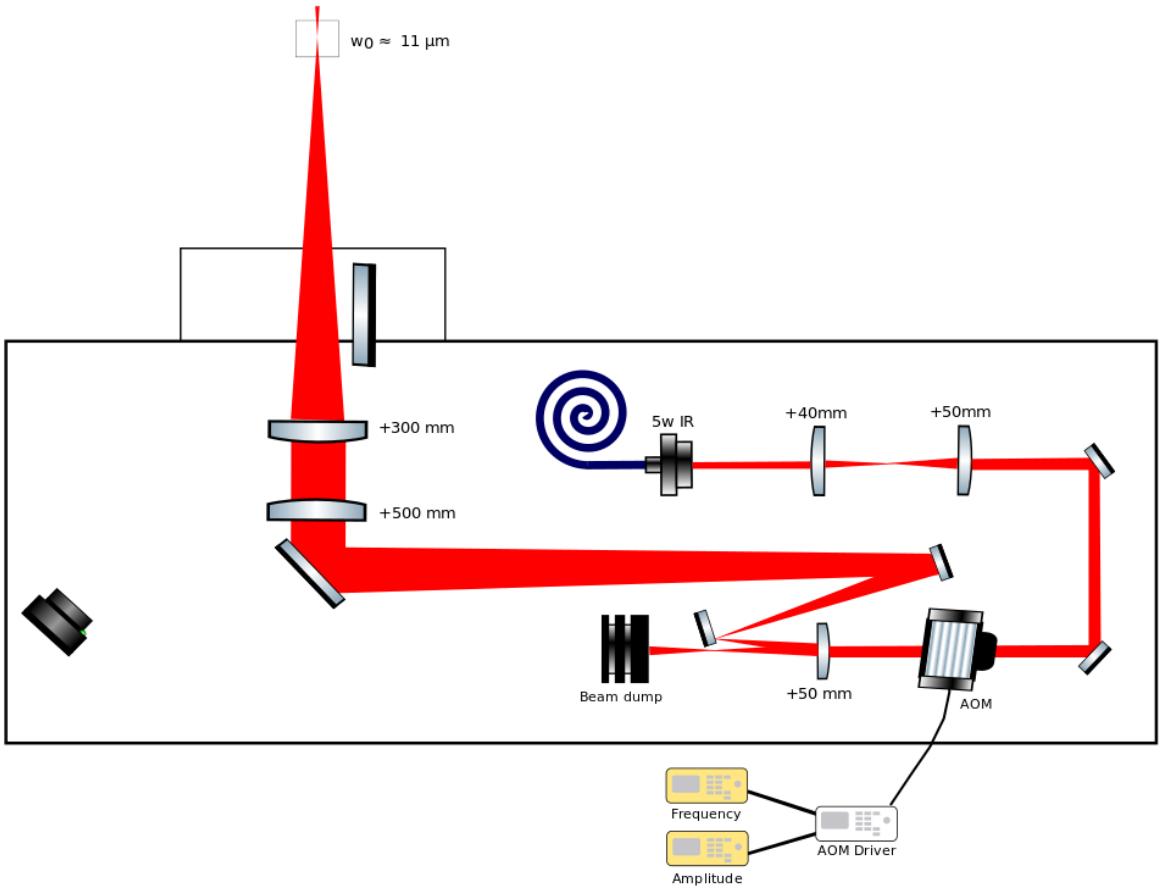

Figure 1: *Schematic of the optical dipole trap setup*

position can also be imaged onto the camera through the same lens. Using this method, the focus of the laser beam can be adjusted and overlapped with the atomic cloud.

3.2.2 Scanning

By varying the AOM frequency with the arbitrary waveform generator, the deflection angle of the first order is varied. This results in a translation of the focus in the experimental chamber. The AOM frequency is scanned from 60 - 110 MHz, resulting in a scanning width of $\sim 10w_0$ in the experimental chamber. A time-averaged potential is created by scanning over 15 points with a frequency of 20 kHz. Each point consists of an approximately Gaussian profile, with a spacing of $\sim 0.7w_0$. For each point the amplitude is corrected using the second arbitrary waveform generator, in order to create a uniform 'sheet potential'.

4 Stationairy Trap

Before trying to create a sheet potential by scanning the AOM frequency, we have to look at the stationairy trap. Section 4.1 covers the beam quality with a determination of the waist size. The measurements done to determine the trap frequencies are discussed in section 4.2. The results of these measurements and a comparison to theory are found in section 4.3. A discussion of these results is found in section 4.4. Measurements to characterize the dipole trap using thermal clouds above the transition temperature are found in Appendix A2.

4.1 Beam quality

After optimizing the optical setup, the beam waist is measured as a function of position. With this we determine the waist size of the focus w_0 and the beam quality factor M^2 as defined in Ref [7]. The size of the focus is in agreement with calculations that were done before building the optical setup and M^2 is close to 1. However, there is astigmatism due to the birefringent crystal in the AOM. Figure 2 shows the horizontal and vertical waist size as a function of position, with w_0 determined from fitting equation (8). The horizontal and vertical foci are separated by a distance of approximately 240 micrometers.

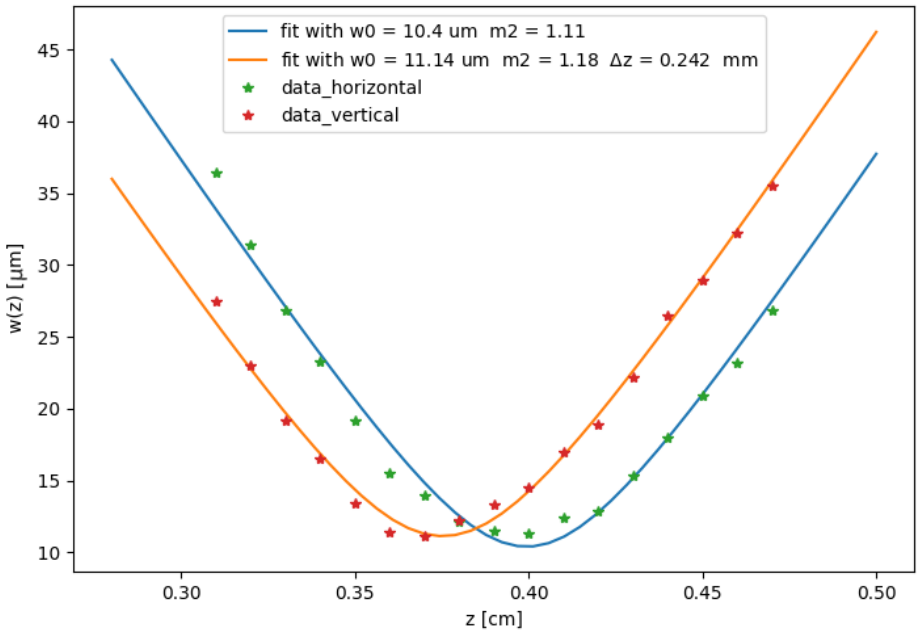

Figure 2: *Beam waist as function of position with fit values.*

Figure 3 is an image of the optical dipole trap in a cloud of thermal (non-condensed) atoms. The laser beam is red-detuned, so the atoms are attracted towards the light field. This results in a higher density of atoms in the optical trap, visualized by the darker blue color.

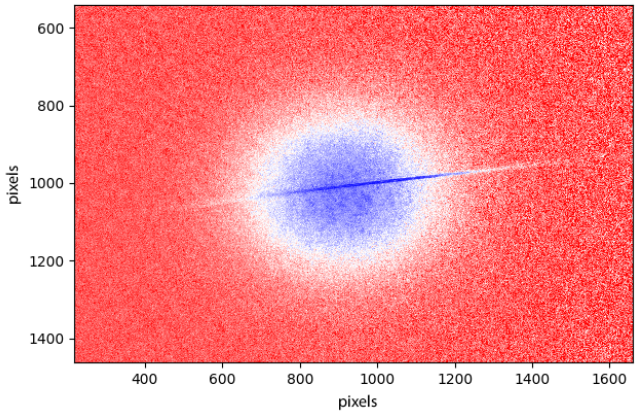

Figure 3: *Optical dipole trap in a cloud of thermal atoms, the pixel size is 3.75 μm.*

4.2 BEC expansion

In order to characterize the trap, we can trap a BEC and release the surrounding atoms by switching of the MT (figure 4).

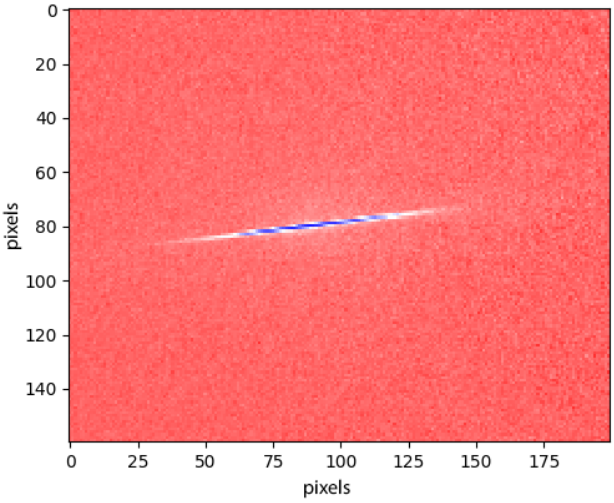

Figure 4: *A BEC in the optical dipole trap, the pixel size is 3.75 μm.*

After turning of the dipole trap itself, the BEC expands due to the conversion of chemical potential to kinetic energy. After Time-Of-Flight (TOF) times of 0, 1, 2, 4, 6, 8, 12, 24, 32 ms we take an image of the condensate. Due to the destructivity of absorption imaging, a new condensate has to be formed for each image. Figure 5 shows one of these images, taken after a TOF of 6 ms.

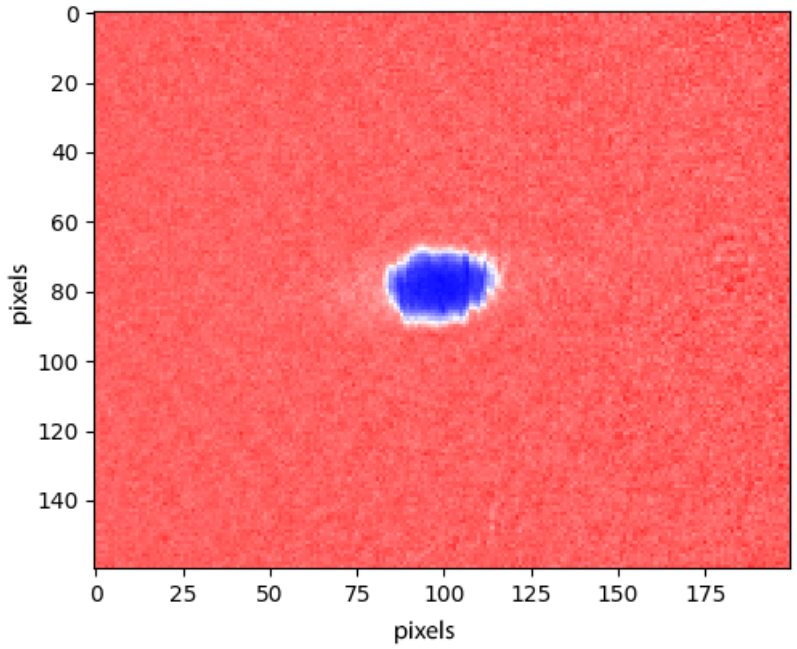

Figure 5: *A BEC after 6 ms TOF.*

By fitting a Thomas-Fermi density distribution model to each image, the radius in the radial direction can be determined. In order to characterize the trap, measurements are done at 4 different laser powers; 9.3 mW, 13.8 mW, 19.0 mW and 24.6 mW. All images can be found in Appendix A, where each column of images represents a different laser power and each row a different TOF. For each of the columns we can calculate the expansion velocity v_{exp}.

4.3 Results

The Thomas-Fermi radius can be plotted as a function of time to estimate the expansion velocity v_{exp} for each laser power. Figures 6.1-6.4 show these plots for each of the series of measurements.

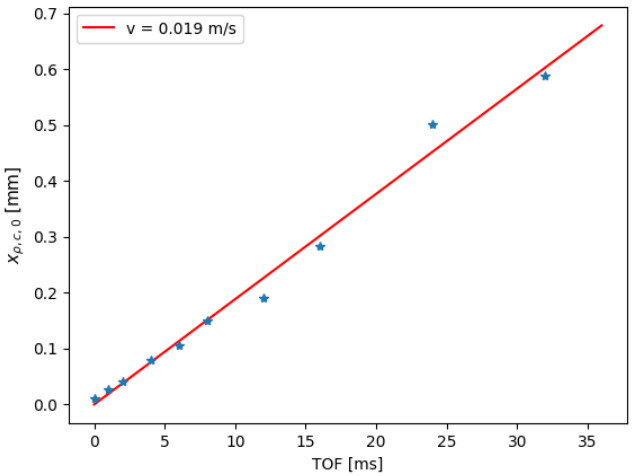

6.1) $x_{\rho,c,0}$ as function of TOF for P=9.3 mW

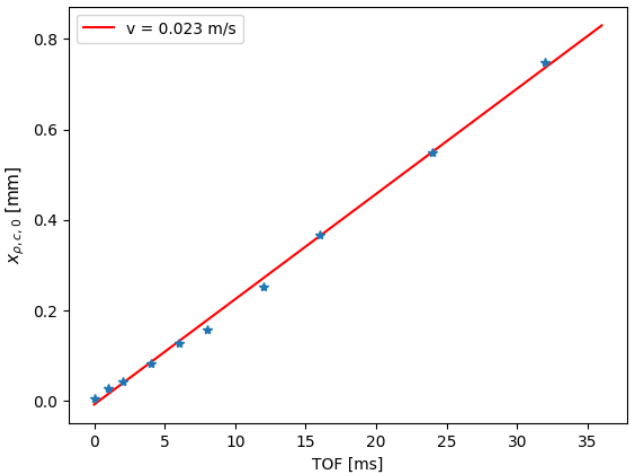

6.2) $x_{\rho,c,0}$ as function of TOF for P=13.8 mW

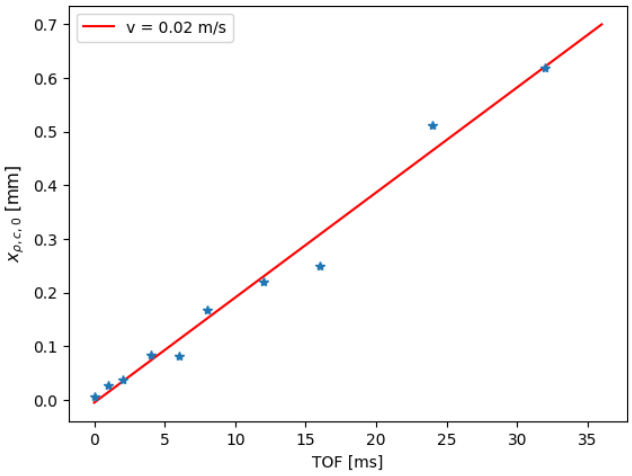

6.3) $x_{\rho,c,0}$ as function of TOF for P=19.0 mW

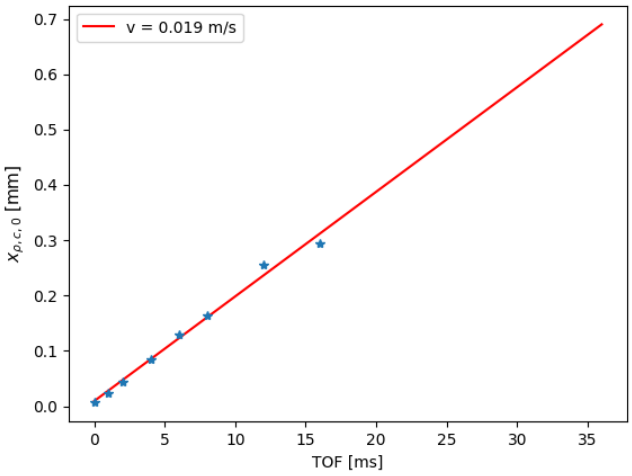

6.4) $x_{\rho,c,0}$ as function of TOF for P=24.6 mW

With this velocity, we can use equation (17) to calculate the chemical potential of the optical dipole trap. Table 1 shows the values for each laser power.

Table 1: *Chemical potential of optical dipole trap*

Laser power	μ
9.3 mW	10.4 kHz
13.8 mW	15.2 kHz
19.0 mW	11.5 kHz
24.6 mW	10.4 kHz

With the chemical potential, equations (15) and (16) can be used to determine the trap frequency for each image. By taking the average over these images, we find the average radial and axial trap frequencies, $\langle\omega_z\rangle$ and $\langle\omega_\rho\rangle$, which are listed in table 2. We can compare these values to the values resulting from equations (10) and (11), using the same values for the laser power and $w_0 = 10.8$ μm, the average of the horizontal and vertical foci. These values, ω_z and ω_ρ, are also listed in table 2.

Table 2: *Measured and calculated trap frequencies of optical dipole trap*

Laser power	$\langle\omega_z\rangle$	ω_z	$\langle\omega_\rho\rangle$	ω_ρ
9.3 mW	$2\pi \cdot 18.1$ Hz	$2\pi \cdot 20.6$ Hz	$2\pi \cdot 1207.0$ Hz	$2\pi \cdot 927.8$ Hz
13.8 mW	$2\pi \cdot 27.4$ Hz	$2\pi \cdot 25.1$ Hz	$2\pi \cdot 1516.7$ Hz	$2\pi \cdot 1130.1$ Hz
19.0 mW	$2\pi \cdot 28.0$ Hz	$2\pi \cdot 29.4$ Hz	$2\pi \cdot 2099.0$ Hz	$2\pi \cdot 1326.1$ Hz
24.6 mW	$2\pi \cdot 30.4$ Hz	$2\pi \cdot 33.5$ Hz	$2\pi \cdot 1641.3$ Hz	$2\pi \cdot 1508.9$ Hz

For a part of the images, the optical density of the condensate is low enough to determine the number of atoms. At 9.3 mW and 13.8 mW this was the case after 8 ms TOF, whilst for 19.0 mW and 24.6 mW the atoms could be counted after 4 ms TOF. Table 3 lists the average number of atoms over these images.

Table 3: *Average number of atoms in dipole trap*

Laser power	$\langle N\rangle$
9.3 mW	$1.35 \cdot 10^6$
13.8 mW	$1.59 \cdot 10^6$
19.0 mW	$4.15 \cdot 10^5$
24.6 mW	$3.72 \cdot 10^5$

4.4 Discussion

The axial trap frequencies determined from the BEC expansion measurements correspond well to the theoretical values for the optical dipole trap (Table 2). The values found for the radial trap frequencies, however, are higher than expected. One possible explanation for this is the fringe pattern that we see in the BEC during expansion. In the images of P=9.3 mW in Appendix A, we clearly see a fringe pattern emerging at TOF=2 ms. This pattern is visible at all laser powers and remains during the entire expansion, possibly accelerating the expansion in the radial direction. The origin of these fringes are suspected to be the inward flow of atoms from both 'ends' of the dipole trap interfering and forming the pattern. A slower transfer from the MT to the dipole trap had no effect in reducing the effects of this fringe pattern.
The number of atoms in the trap seems to decrease when the laser power is increased (Table 3). This can be explained by increasing three-body losses at higher intensities. The decreasing number of atoms in turn explain why the chemical potential of the condensate does not increase for higher laser powers.

5 Scanned Trap

Section 5.1 introduces the scanning method. The optimization algorithm is explained in section 5.2, followed by the results in section 5.3. These results are discussed in section 5.4.

5.1 Scanning

By rapidly scanning the focus, we attempt to create a uniform sheet potential. We do this by scanning over 15 points with ∼150 mW of laser power, with a spacing between the points of approximately $0.7 \cdot w_0$. With a scanning frequency of 20 kHz, the atoms see a time-averaged potential. The scanned trap is imaged on the camera with the folding mirror. When we set the AOM amplitude constant at the maximum value and scan the frequency from 60 to 110 MHz, we observe the image shown in figure 7 on the camera.

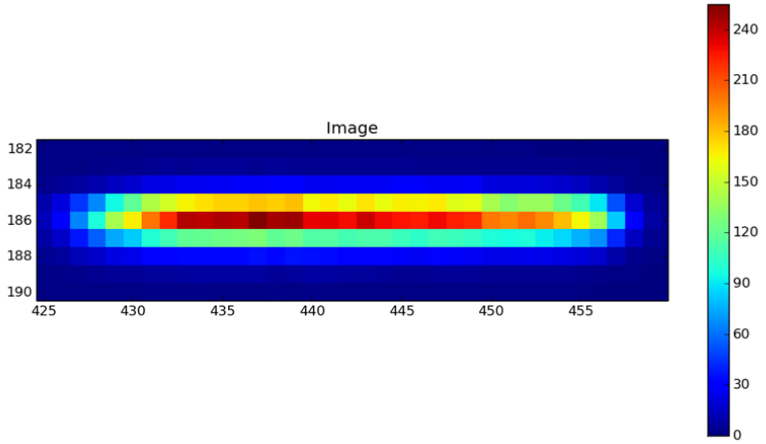

Figure 7: *Camera image of scanned focus at constant amplitude*

The width of the scan is approximately 30 pixels, which is equal to 112.5 μm $\approx 10 \cdot w_0$. If we make a cut through pixel-row 186, we see the intensity profile shown in figure 8.

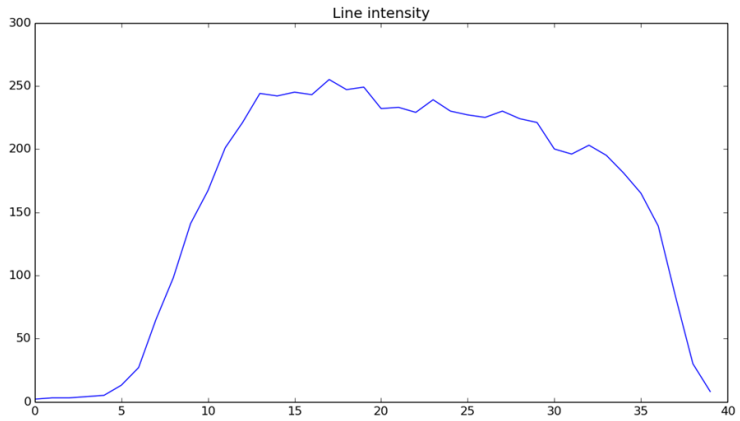

Figure 8: *Intensity profile of pixel-row 186*

5.2 Optimization

To create a quasi-2D sheet of BEC atoms, we have to create a homogeneous potential. This will obviously not work with a constant amplitude, as the AOM efficiency decreases as the deflection angle increases. We compensate this efficiency loss by increasing the AOM amplitude for larger deflection angles and lowering the amplitude in the center of the scan. As a starting point, we take an image of each of the 15 individual points in the scan. Figure 9 shows the result of this at a constant amplitude.

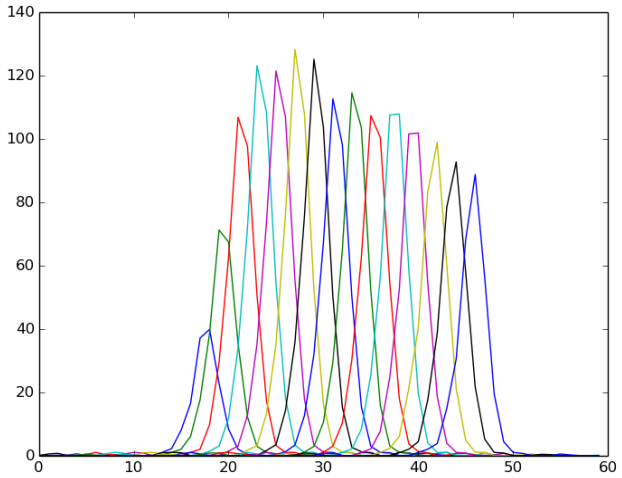

Figure 9: *Individual scanning points at maximum amplitude*

An algorithm fits a Gaussian to each of these points to determine the position of each of the peaks. The algorithm tries to create a flat potential by moving the peaks (with a limit of 1 pixel in each direction) and changing the amplitude. The first iteration of this algorithm is shown in figure 10. The red dots indicate the intensity on the pixels of the camera before the optimization. The black dots are the new intensities on the pixels and the black curves are the Gaussian fits to the corrected amplitudes at the newly chosen positions. These black curves add up to the red line. So the algorithm tries to put the black dots on the red line, optimizing the flatness of the sheet potential.

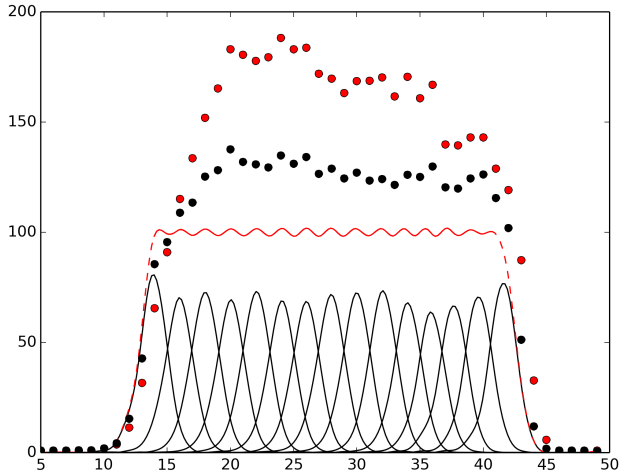

Figure 10: *First iteration of the optimization algorithm. Red dots indicate the intensity on the camera pixels before optimization, the black dots after optimization. The black curves are Gaussian fits to the new peaks at the new positions. The red line is the sum of these black curves.*

After roughly 10-15 iterations, the algorithm fails to improve the potential further. The amplitude and frequency configuration of each iteration is saved, so we can choose the best configuration and reload it in the arbitrary waveform generators. If we for instance reload the 13th iteration, which is shown in figure 11, we have a resulting line intensity on the camera shown in figure 12.

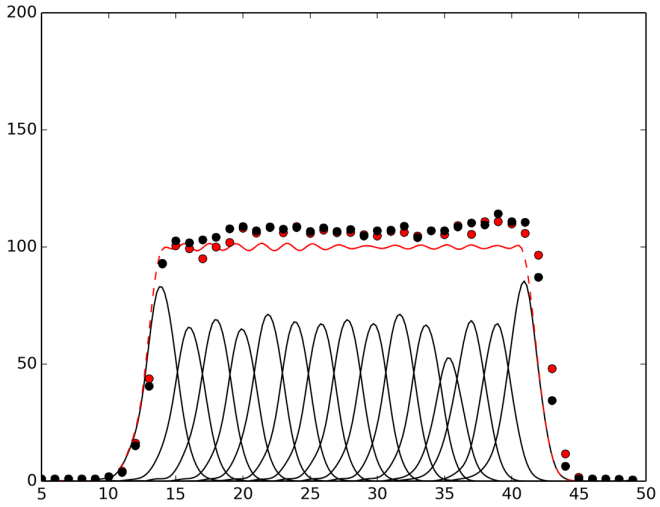

Figure 11: *13th iteration of the optimization algorithm.*

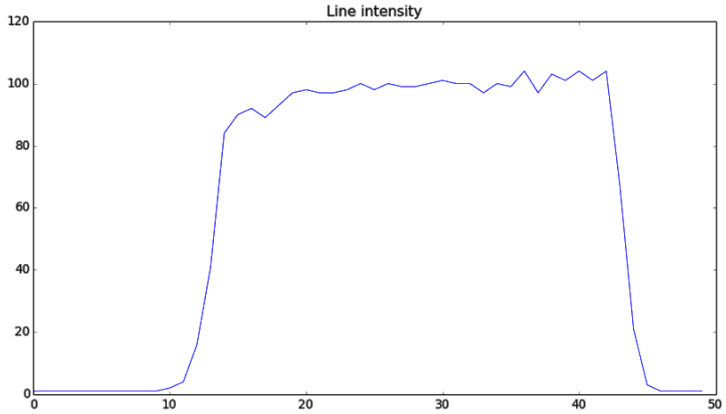

Figure 12: *Line intensity on camera using the 13th iteration of the optimization algorithm.*

The intensity variations are still on the order of ∼5%, which is too large for a smooth potential. The BEC will therefore spread in the individual peaks of the potential. To see what the result of such a potential is on a BEC, we used the - relatively flat - configuration iteration shown in figure 13 and imaged this on the atoms.

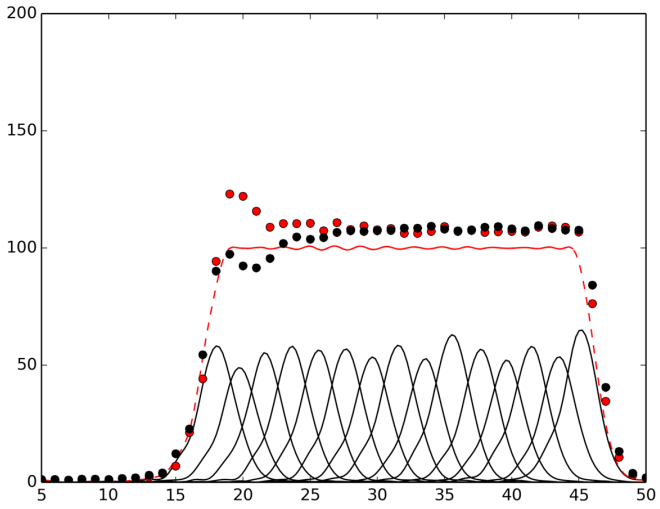

Figure 13: *Configuration used on the BEC in images 14 and 15.*

5.3 Results

Figures 14 and 15 show images of a BEC in the scanned dipole trap. In figure 14 the MT was switched off for 20 ms before taking the image, whilst in figure 15 it was off for 150 ms before taking the image.

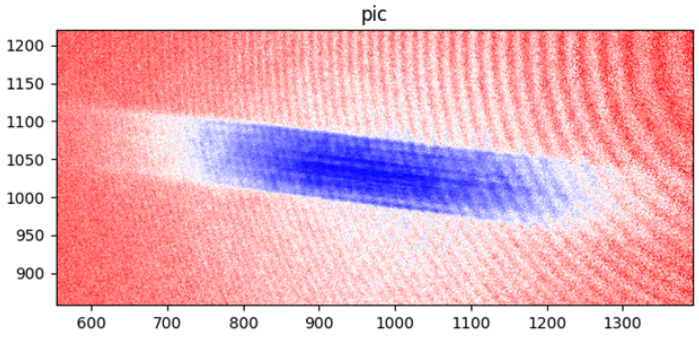

Figure 14: *BEC in scanned optical dipole trap 20 ms after switching off the MT*

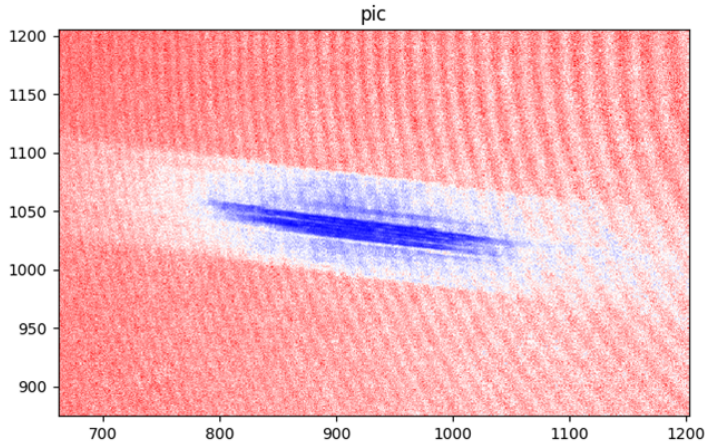

Figure 15: *BEC in scanned optical dipole trap 150 ms after switching off the MT*

5.4 Discussion

As seen in chapter 4, the trap frequencies are sufficient to trap a BEC. We furthermore see that both the width and speed of the scan are sufficient to create a wide quasi-2D sheet of BEC atoms. But due to a too large variation in the intensity profile of the sheet potential, the BEC will not distribute evenly throughout the potential. The optimization algorithm fails to find a set of scanning amplitudes and frequencies that will result in a uniform potential. Possible improvements to achieve a quasi-2D BEC are discussed in chapter 6.

6 Conclusion & Outlook

We are able to repeatedly trap and hold BECs in the stationairy optical dipole trap. The trap frequencies determined by expanding these BECs from the trap correspond well to theoretical predictions. The measured radial trap frequencies are slightly higher than the calculated values. This might be explained by the observed fringe pattern in the expanding BEC. A slower transfer from the MT to the dipole trap did not resolve this fringe pattern.

By scanning the AOM frequency, we attempted to create a uniform sheet potential. The scanning is fast enough and reaches a width of $\sim 10 \cdot w_0$. We have more than enough laser power to scan over the number of points necessary to create a flat potential, which is already shown in Ref [8]. However, the sheet trap has too large intensity variations to create an evenly distributed quasi-2D BEC.

More measurements are needed to explain the fringe pattern that appears in the expanding BEC. There might be a way to prevent these fringes in the BEC when the cause is known. This would enable a more accurate characterization of the dipole trap. The cause of these fringes might also interfere with the optimization of the sheet potential.

Currently, the optimization algorithm of the scan is altered in order to decrease the variations in the intensity profile. There is also room for improvement in the beam quality. The M^2 values are close to 1, but can be further decreased to improve the Gaussian beam profile. Another possible improvement is to compensate for the astigmatism that results from the birefringent crystal in the AOM with a cylindrical lens.

7 Acknowledgements

I want to thank Jasper for always making time to help out with my project, for his endless enthusiasm for experimental physics and for listening to tropical house in a dark lab whilst wearing laser glasses. I want to thank Peter for his guidance and for keeping hope alive when we faced yet another problem, or maybe a factor of 2π. Sanne, thank you for also being a master student in the same group at the same time and for sharing both Jasper time and lab time. I also want to thank Dante, Paul, Cees and Frits (on Tuesdays) for their technical support. Finally, i want to thank the entire nanophotonics group for a great year.

References

[1] M. H. Anderson, J. R. Ensher, M. R. Matthews, C. E. Wieman and E. A. Cornell, Science, 269(5221):198–201 (1995)

[2] K. B. Davis, M. O. Mewes, M. R. Andrews, N. J. van Druten, D. S. Durfee, D. M. Kurn and W. Ketterle, Phys. Rev. Lett. **75**, 3969 (1995)

[3] S. Loth, MSc thesis, Utrecht University (2018)

[4] R. Grimm, M. Weidemüller and Y. Ovchinnikov, arXiv:physics/9902072 (1999)

[5] W. Ketterle, D.S. Durfee and D.M. Stamper-Kurn, arXiv:cond-mat/9904034 (1999)

[6] Y. Castin and R. Dum, Phys. Rev. Lett. **77**, 5315 (1996)

[7] A. E. Siegman, OSA TOPS Vol. 17, MQ1 (1998)

[8] T. A. Bell, J. A. P. Glidden, L. Humbert, M. W. J. Bromley, S. A. Haine, M. J. Davis, T. W. Neely, M. A. Baker, H. Rubinsztein-Dunlop, New J. Phys. **18** 035003 (2016)

A Appendix

A.1 Time-Of-Flight expansion of BEC's

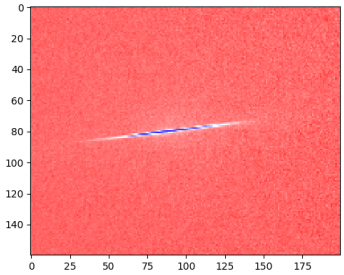

TOF=0 ms, P=9.3 mW

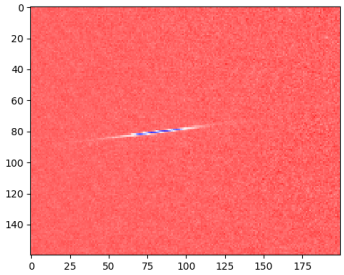

TOF=0 ms, P=13.8 mW

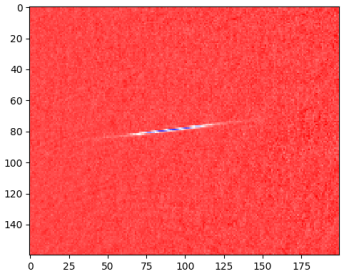

TOF=0 ms, P=19.0 mW

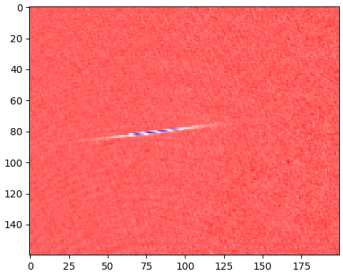

TOF=0 ms, P=24.6 mW

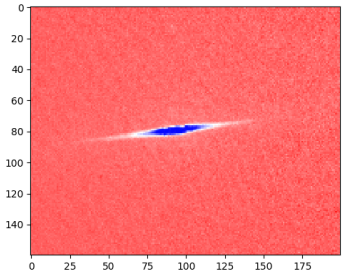

TOF=1 ms, P=9.3 mW

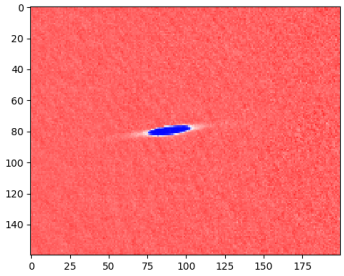

TOF=1 ms, P=13.8 mW

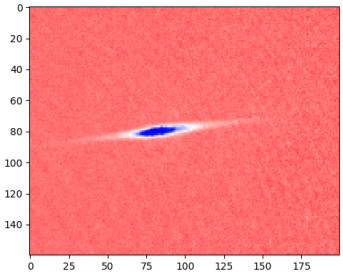

TOF=1 ms, P=19.0 mW

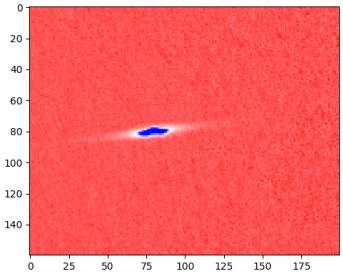

TOF=1 ms, P=24.6 mW

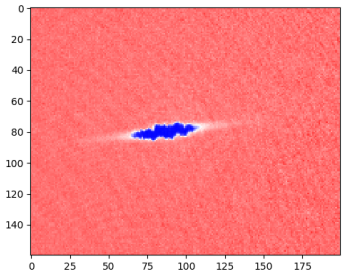

TOF=2 ms, P=9.3 mW

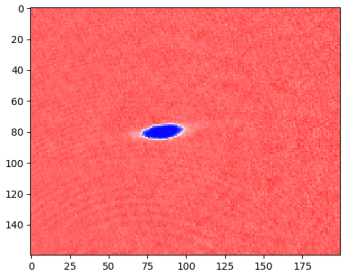

TOF=2 ms, P=13.8 mW

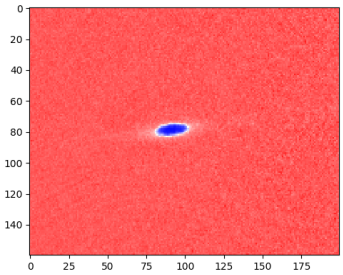

TOF=2 ms, P=19.0 mW

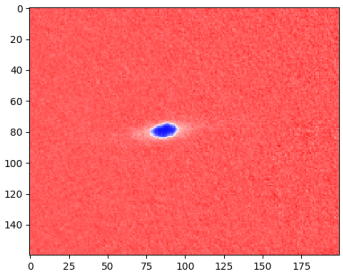

TOF=2 ms, P=24.6 mW

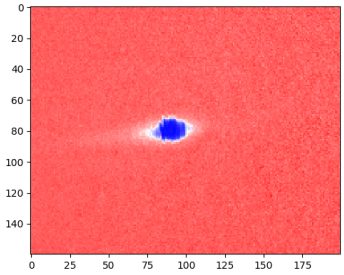

TOF=4 ms, P=9.3 mW

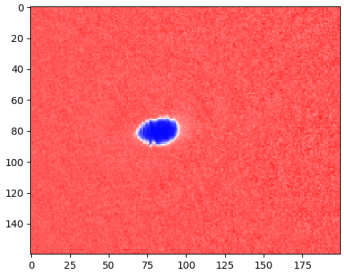

TOF=4 ms, P=13.8 mW

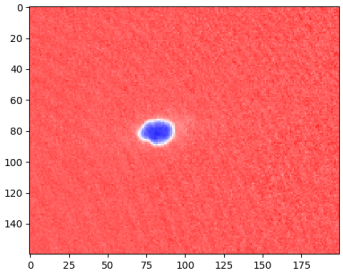

TOF=4 ms, P=19.0 mW

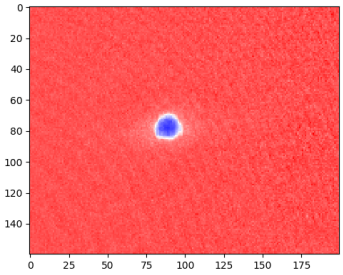

TOF=4 ms, P=24.6 mW

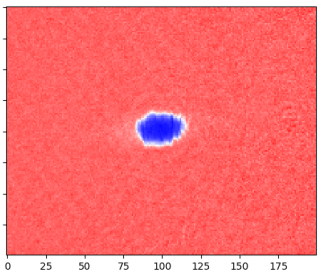

TOF=6 ms, P=9.3 mW

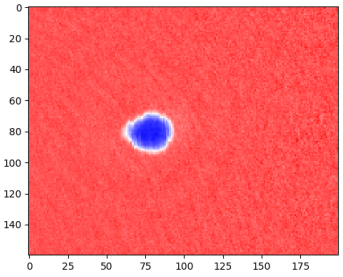

TOF=6 ms, P=13.8 mW

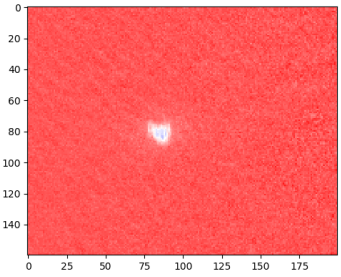

TOF=6 ms, P=19.0 mW

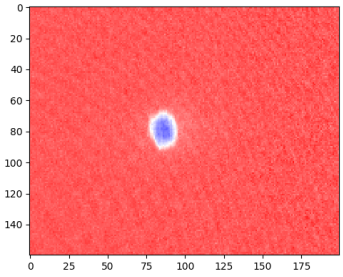

TOF=6 ms, P=24.6 mW

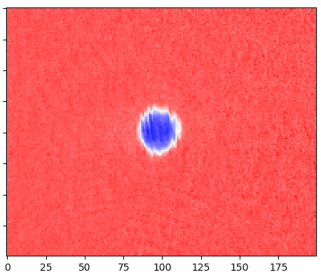

TOF=8 ms, P=9.3 mW

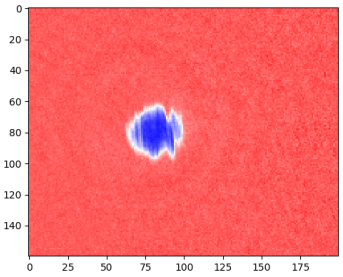

TOF=8 ms, P=13.8 mW

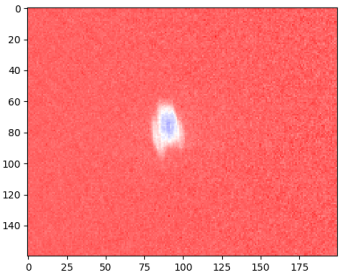

TOF=8 ms, P=19.0 mW

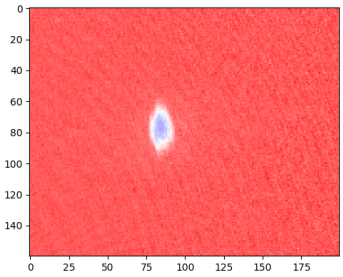

TOF=8 ms, P=24.6 mW

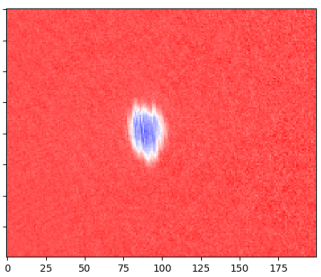

TOF=12 ms, P=9.3 mW

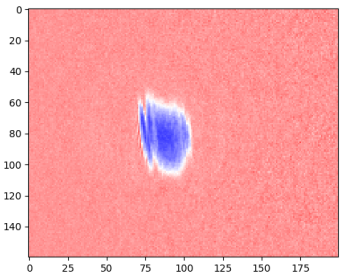

TOF=12 ms, P=13.8 mW

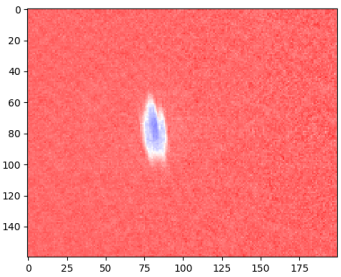

TOF=12 ms, P=19.0 mW

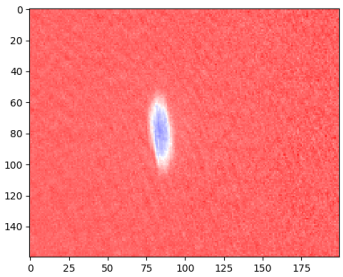

TOF=12 ms, P=24.6 mW

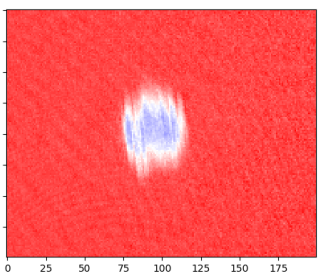

TOF=16 ms, P=9.3 mW

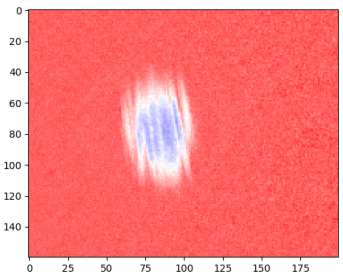

TOF=16 ms, P=13.8 mW

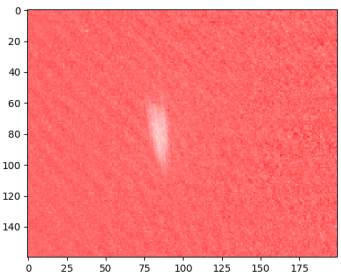

TOF=16 ms, P=19.0 mW

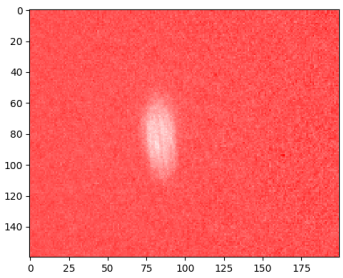

TOF=16 ms, P=24.6 mW

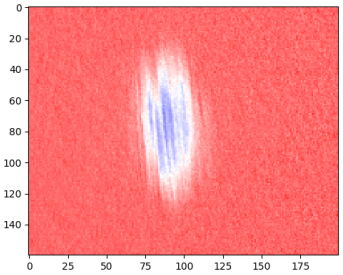

TOF=24 ms, P=9.3 mW

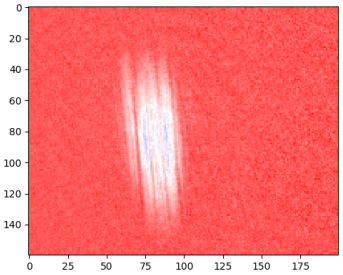

TOF=24 ms, P=13.8 mW

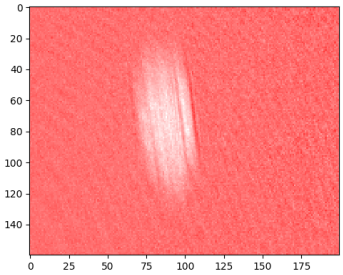

TOF=24 ms, P=19.0 mW

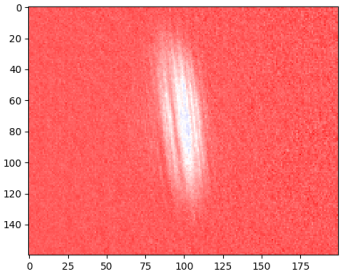

TOF=32 ms, P=9.3 mW

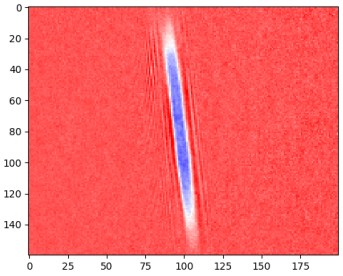

TOF=32 ms, P=13.8 mW

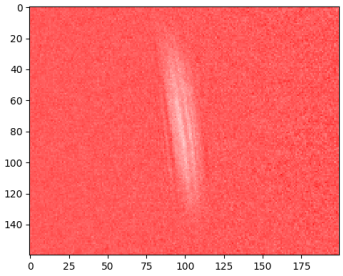

TOF=32 ms, P=19.0 mW

A.2 Measurements above the transition temperature

A.2.1 Temperature

To further investigate the behavior of the optical trap, images were taken of the expansion of a thermal cloud above the BEC transition temperature. This was done at laser powers of 155 mW, 233 mW, 326 mW, 424 mW and 521 mW. The images were taken after a TOF interval of 0 ms, 3 ms, 6 ms, 9 ms, 12 ms and 15 ms after turning off the optical trap. By fitting a Gaussian distribution, the radius of the thermal cloud in the radial direction was determined. The temperature of the thermal cloud was calculated by fitting the following equation [5]:

$$\sigma_x(t) = \sqrt{\sigma_{x,0}^2 + \frac{K_B T}{m} t^2}, \tag{18}$$

with $\sigma_x(t)$ the radius at a TOF time t, σ_{x0} the radius at TOF = 0 (a free parameter in the fit) and T the temperature. The results of these measurements are found in figures 16.1 - 16.5, the resulting temperatures as function of laser power are found in figure 16.6.

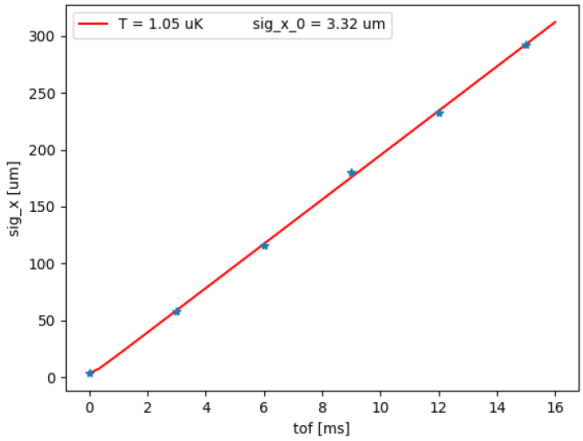

16.1) σ_x as function of TOF for P=155 mW

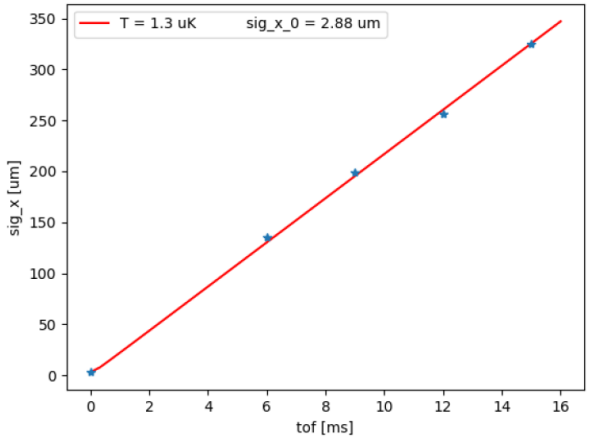

16.2) σ_x as function of TOF for P=233 mW

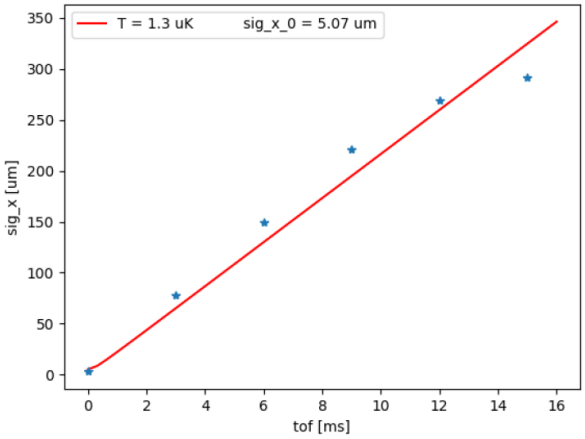

16.3) σ_x as function of TOF for P=326 mW

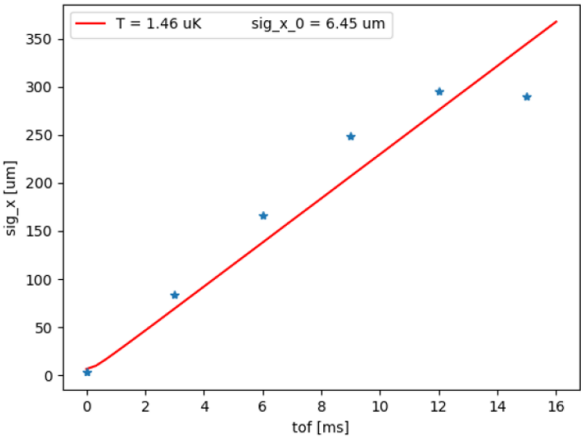

16.4) σ_x as function of TOF for P=424 mW

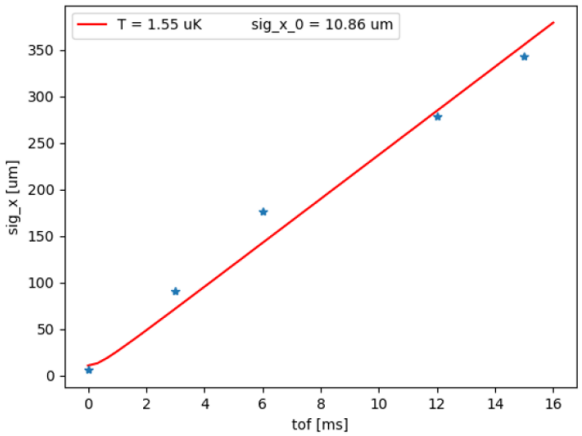

16.5) σ_x as function of TOF for P=521 mW

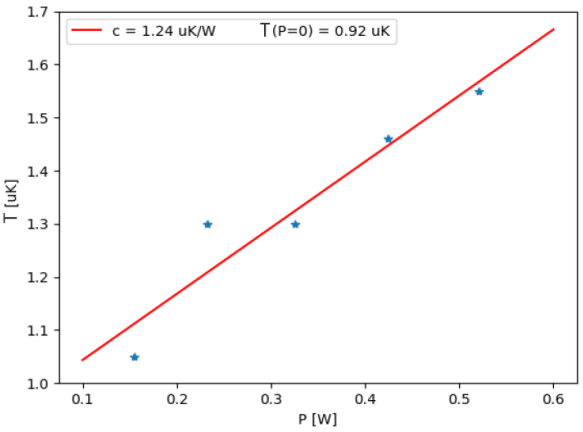

16.6) Temperature T as function of laser power

As the number of particles in the trap increases for higher powers, the measured width in the radial direction also increases. We also note that $\sigma_x(t)$ is smaller than the waist size w_0. This is due to the atoms being trapped in the bottom of the potential, having a small radial and axial extension compared to the trap dimensions.

A.2.2 Number of particles

Figures 17.1 - 17.5 show the number of atoms as function of the time-of-flight (TOF). Figures 17.6 and 17.7 show the number of atoms as function of laser power at TOF=0 ms and TOF=12 ms. We see that the number of particles in the trap at TOF=0 ms increases when the laser power is increased, but at TOF=12 ms we are left with fewer particles if we increase the laser power. The number of trapped atoms is larger for higher laser powers, but they are lost faster in the expansion. This can be explained by the increase of three-body losses at higher intensities.

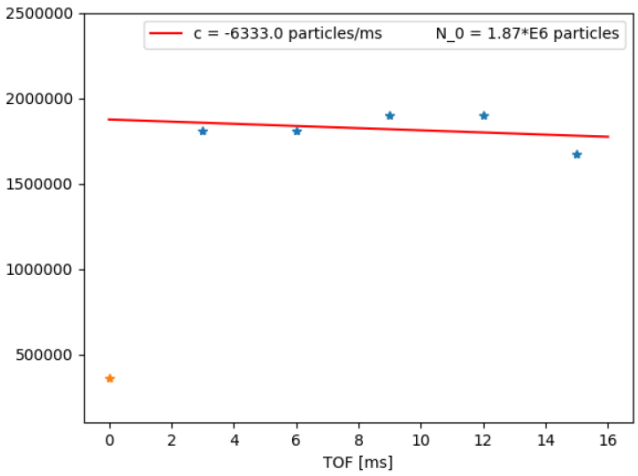

17.1) Number of atoms as function of TOF for P=155 mW

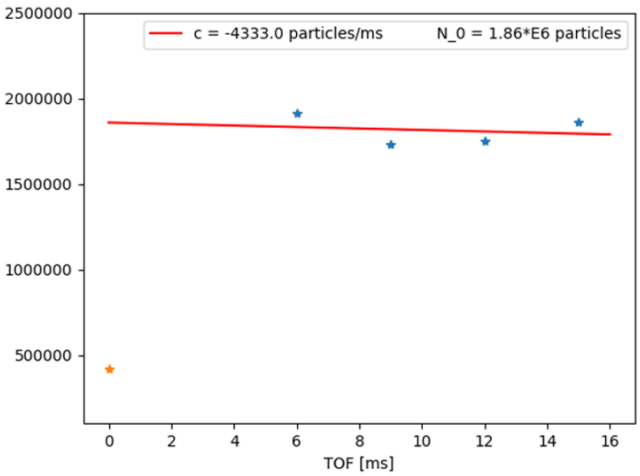

17.2) Number of atoms as function of TOF for P=233 mW

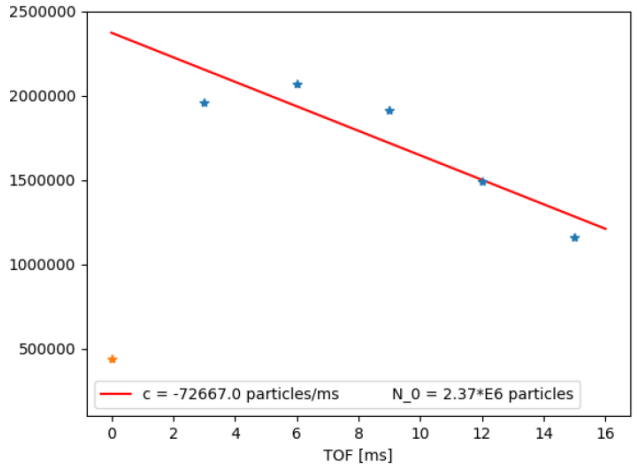

17.3) Number of atoms as function of TOF for P=326 mW

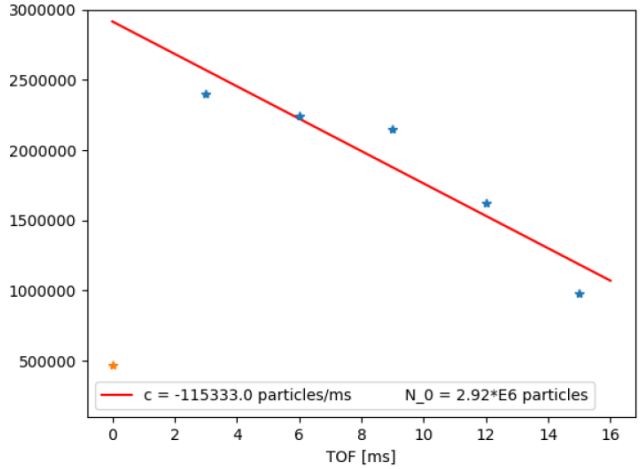

17.4) Number of atoms as function of TOF for P=424 mW

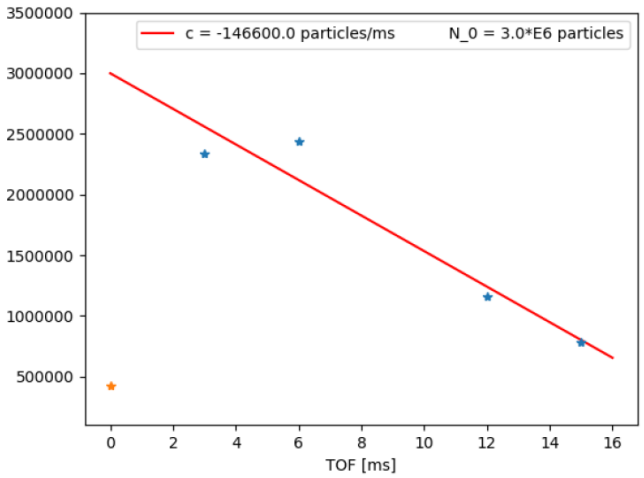

17.5) Number of atoms as function of TOF for P=521 mW

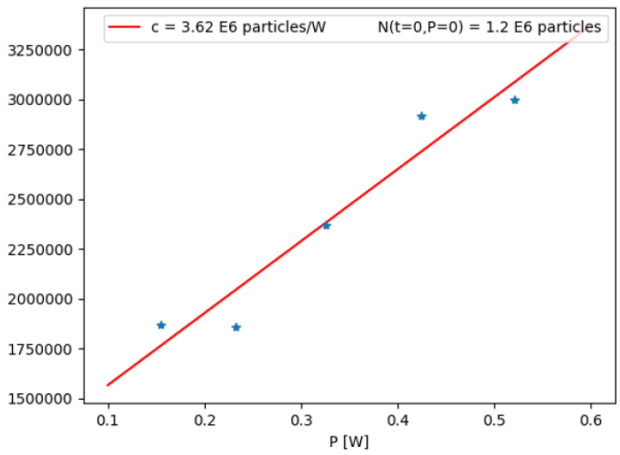

17.6) Number of atoms as function of power at TOF=0 ms

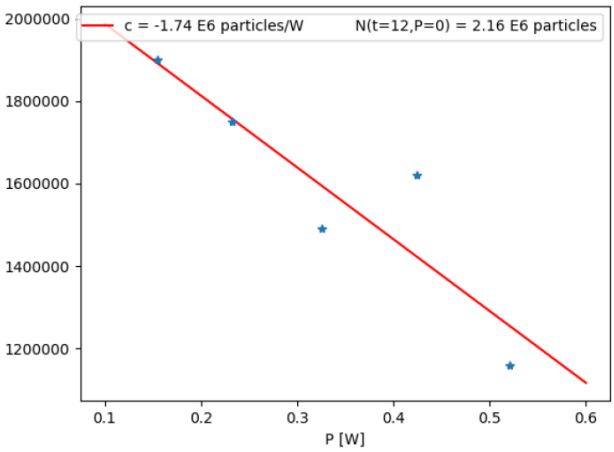

17.7) Number of atoms as function of power at TOF=12 ms